Thermal feedback on wind-stress as a contributing cause of climate variability

Paola Cessi

Scripps Institution of Oceanography, La Jolla, CA 92093, U.S.A.

November 30, 1999

Corresponding author address: Paola Cessi, Scripps Institution of Oceanography, UCSD-0230, La Jolla, CA 92093-0230 (e-mail: pcessi@ucsd.edu)

ABSTRACT

A model which isolates the interaction between midlatitude ocean gyres and the wind-stress due to atmospheric baroclinic eddies is formulated. The ocean and atmosphere are coupled through their respective heat balances and global heat and momentum conservations are enforced. The ocean flow creates a steep oceanic thermal front at the midlatitude intergyre boundary. This frontogenesis sharpens the atmospheric temperature gradients and locally increases the atmospheric eddy heat transport. The result is a well defined storm-track, which, because of the delayed adjustment of the gyres to the wind-stress, oscillates in time with a period of about eighteen years.

1. Introduction

Recent estimates of Trenberth and Solomon (1994) indicate that the poleward heat transport in the Northern hemisphere's Pacific ocean peaks at about 1×10^{15}W. This represents about half of the maximum total meridional heat transport carried by the oceans in the Northern Hemisphere. The other half of the oceanic poleward heat transport is carried by the North Atlantic. The indirect estimate obtained by Trenberth and Solomon (1994) agrees, within uncertainties, with the heat flux calculations based on direct ocean measurements (e.g. MacDonald and Wunsch, 1996 and Bryden et al., 1991).

The partition of the ocean meridional heat flux into different ocean basins allows some insight into different modes of meridional heat transport: very little thermohaline transport occurs in the North Pacific, so we can consider all of the meridional heat flux in the North Pacific to be carried by the wind-driven flow. The partition of the Atlantic northward heat flux between the thermohaline and wind-driven flow is presently unclear.

For reference, the maximum zonally averaged heat flux transported by the atmosphere in the Northern hemisphere is about 4×10^{15}W. Thus, even if the North Atlantic heat transport were entirely due to the thermohaline cell, the wind-driven circulation in the Pacific is responsible for a considerable fraction of the global heat budget.

Bjerknes (1964) suggested that fluctuations in the mid-latitude winds lead to changes in the wind-driven ocean currents which affect the wind-driven poleward heat transport by the ocean. Because of the decadal time scale of adjustment for the upper-ocean wind-driven flow, the atmosphere can be assumed to be in equilibrium with the radiative forcing, and the changes in the ocean heat transport must be compensated by changes in the atmospheric heat transport. Thus the atmospheric circulation, including the surface wind-stress, is affected by the oceanic variability and the interaction between the midlatitude atmosphere and the ocean has the potential for producing low-frequency fluctuations.

The heuristic arguments offered by Bjerknes (1964) are quantified here by formulating a model which isolates the interaction between the wind-driven ocean flow and the wind-stress, via global conservation of heat and momentum.

The motivation for the model formulation comes mostly from results of atmospheric general circulation models (AGCM) aimed at understanding the midlatitude atmospheric response to persistent sea surface temperature (SST) deviations from climatological values. Unfortunately, computations performed with different models have given inconsistent results (cf. Palmer and Sun 1985; Pitcher et al. 1988, Peng et al. 1995). The differences among the results of the numerical experiments reported in the literature are mostly in the *vertical* penetration of temperature anomalies into the upper troposphere, and in the *longitudinal* distribution of the geopotential response. Kushnir and Held (1996) provide a concise summary of the discrepancies among different AGCMs.

The one robust feature that emerges from the better resolved numerical experiments (Palmer and Sun 1985; Ferranti et al. 1994) is that SST anomalies result in the meridional displacement of storm-tracks. Support for this result also comes from the diagnostic study of Hoskins and Valdes (1990), which shows that the diabatic heating provided by the warm SST in the western boundary current extension regions, off the eastern coast of midlatitude continents, is essential for the maintenance of the storm-track.

Inspired by the aformentioned studies, we conjecture that the main role of sea surface temperatures is to contribute to the mean distribution of atmospheric temperatures upon which mid-latitude baroclinic eddies draw their kinetic energy, and the latter determines the surface wind-stress that drives the ocean circulation. In turn, the upper ocean circulation is responsible for the advection of SST's and for the wind-driven northward heat transport.

Perhaps the simplest setting in which the coupled dynamics of the wind-stress and the wind-driven flow can be studied is by coupling two fundamental models of the separate atmosphere and ocean system: that is, Green (1970) and the time-dependent, baroclinic version of Stommel's (1948) model considered by Veronis and Stommel (1956) and Anderson and Gill (1975).

Given the zonally averaged atmospheric temperature, the meridional heat and momentum fluxes due to baroclinic eddy transport can be calculated using the parametrizations of

Green (1970). The zonally averaged wind stress is then determined by the divergence of the momentum flux. Given the wind stress, Stommel's (1948) model allows us to determine the currents in the upper ocean. The zonally averaged temperature in the atmosphere is then determined by considering the heat budget of the combined ocean-atmosphere's system. In the next section we detail the formulation of these coupled dynamics.

2. The atmospheric budget

On time-scales longer than one month, the atmosphere adjusts "instantaneously" to changes in the ocean, even though the latter evolves in time. That is to say, the atmospheric variables are "fast", so that the atmosphere is enslaved to the slower evolution of the ocean. This does not in any sense mean that the atmosphere is passive: in mid-latitudes, atmospheric baroclinic eddies are essential for the heat, moisture and momentum budget of the Earth; these three quantities determine the heat-flux into the ocean and the wind-stress driving the upper ocean currents. Thus on long time-scales the atmosphere is a slave to the ocean, but it is a hard working slave.

Given the present lack of understanding of the detailed *vertical* and *longitudinal* structure of the atmospheric response to changes in the ocean temperature, our strategy is to focus on the vertically and zonally averaged heat and momentum budget for the atmosphere. Closely following the pioneering work of Green (1970), the zonally averaged wind-stress and the zonally averaged heat flux into the ocean are obtained in terms of a single atmospheric variable, viz. the zonally averaged atmospheric temperature at the surface, $\theta_s(y,t)$.

a. The heat balance

The zonally and vertically averaged heat budget for the atmosphere, assuming equilibrium on the time scales of oceanic evolution, is given by

$$c_{pa}\partial_y \int_0^\infty \rho\overline{(\theta v)}\,\mathrm{d}z = Q_i - Q_o - r\overline{F_0}. \tag{2.1}$$

Here, Q_i is the zonally averaged net absorbed short-wave heat flux at the top of the atmosphere: this is one of the externally prescribed forcings in the system, and it is taken as a specified function of latitude, y. θ indicates the atmospheric potential temperature.

Q_o is the zonally averaged outgoing longwave radiation, which is estimated using a "gray Stefan-Boltzmann law", $Q_o = G(\theta)\,\sigma\theta^4$, linearized around a mean value, Θ (in Kelvins), as is customary in energy balance models. Thus, with $\theta_s(y,t)$ the zonally averaged atmospheric surface temperature, the outgoing long wave radiation is approximated by:

$$Q_o = A + B\theta_s, \tag{2.2}$$

with A and B prescribed constants.

Throughout the article, the overline indicates zonal average, so that $\overline{F_0}$ is the zonally averaged heat flux at the interface between the atmosphere and the ocean. Clearly the contribution of F_0 to the atmospheric heat balance must be weighted by the fraction of latitude circle, r, occupied by the ocean basins. Several processes, such as emitted long wave radiation, latent and sensible heat contribute to the air-sea fluxes. For the limited range of temperatures found on the earth's surface, it is possible to linearize the formulas used for calculating the heat fluxes around a prescribed state (Haney 1971):

$$F_0 = \mathcal{F}(y) + \lambda(\theta_s - T_s). \tag{2.3}$$

$\mathcal{F}$ is the portion of the heat flux independent of the air-sea temperature difference (e.g. the short wave radiative flux across the ocean surface), and λ is a bulk transfer coefficent which we approximate with a constant. Together with Q_i, $\mathcal{F}$, is taken as a specified function of latitude, y, and these two fluxes are the only externally prescribed forcings in the whole coupled system.

Finally, ρ is the density of the atmosphere, assumed here to be a function of z only, and $\overline{\theta v}$ is the zonally averaged heat flux. The fundamental assumption made here is that the northward eddy heat transport is dominated by baroclinic eddies, so that $\overline{\theta v} \approx \overline{\theta' v'}$, where the prime indicates departure from the zonal average. Implicit in this approximation is the neglect of heat transport by the zonally averaged circulation. Clearly, this approximation is incorrect in low latitudes, but works well for quasi-geostrophic, midlatitude flow.

Baroclinic eddies are parametrized as proposed by Green (1970):

$$\overline{\theta' v'} = -\kappa \partial_y \overline{\theta}. \tag{2.4}$$

All the hypotheses about the details of the transport processes are encapsulated in the specification of the coefficient of eddy diffusivity, κ. Green (1970), Held (1978) and Branscome (1983) use three different methods to estimate the effective diffusivity due to baroclinic eddies: conservation of energy, mixing length arguments and an explicit calculation of the growth and subsequent equilibration in a specific model of baroclinic eddy development. All three methods, at least in the quasi-geostrophic context, lead to the result that κ depends on $\partial_y \overline{\theta}$ and on z, although the explicit functional forms differ somewhat in the three treatments.

At any rate, here a minimalist approach will be taken, by assuming

$$\kappa = \kappa_s \exp(-z/d), \tag{2.5}$$

with the amplitude, κ_s, and the vertical scale, d, of the eddy diffusivity both constant. Nevertheless, it should be clear that this extreme simplification is provisional, and that the generalization to the more complete parametrizations proposed by Branscome (1983) and successfully tested against three-dimensional simulations by Stone and Yao (1987, 1990) does not pose any essential difficulty. Also, the specific vertical structure for κ is not crucial, because κ and its derivative always appear inside integrals over the depth of the whole atmosphere.

In order to calculate the vertically integrated heat flux, it is necessary to posit a relation between the zonally averaged potential temperature at the surface, $\theta_s(y,t)$, and in the rest of the troposphere, $\bar{\theta}(y,z,t)$. Given that all the parametrization of baroclinic eddies are obtained in the quasi-geostrophic context, we separate the basic stratification,

S, from the dynamical part of the potential temperature, and assume that the latter is independent of height, so that

$$\bar{\theta}(y, z, t) = Sz + \theta_s(y, t). \tag{2.6}$$

Here, for simplicity, we also take S to be constant.

The vertical structure of the atmospheric density is $\rho = \rho_s \exp(-z/D)$, with the scale height, D, a constant. The thermodynamic balance is given by

$$-c_{pa}\rho_s\kappa_s d_e {\partial_y}^2\theta_s = Q_i(y) - A - B\theta_s - r[\mathcal{F}(y) + \lambda(\theta_s - \overline{T_s})], \tag{2.7}$$

where the effective scale-height d_e is defined as

$$d_e \equiv dD(D+d)^{-1}. \tag{2.8}$$

With the specification of no-flux boundary conditions at the boundaries, and knowledge of the sea surface temperature, T_s, (2.7) controls the heat budget of the atmosphere in terms of the zonally averaged atmospheric surface temperature, θ_s, which is a function of latitude and time only. The determination of the sea surface temperature, T_s, is described in section 3.

b. The momentum balance

Closely following Green (1970), it is possible to relate the *zonally averaged* mechanical stress that forces the wind-driven currents to the mean atmospheric temperature gradients. Although, the zonal average is not the whole stress, it is a considerable fraction of what forces the large-scale currents in planetary basins, such as the North Pacific.

The *zonally* averaged $x-$component of the wind-stress, τ, is

$$\tau = -\partial_y \int_0^\infty \rho\overline{(u'v')}\,\mathrm{d}z. \tag{2.9}$$

Again the overline indicates a zonal average; (2.9) is an exact result in statistical steady state. The mixing length arguments leading to the relation (2.4) between the eddy heat flux and the mean temperature gradient cannot be used to estimate directly the momentum flux, because momentum is not conserved following particles. Green (1970) uses the quasigeostrophic approximation to relate the eddy momentum flux, $\overline{u'v'}$, to the eddy fluxes of heat, $\overline{\theta'v'}$, and potential vorticity, $\overline{q'v'}$, so that:

$$\partial_y(\overline{\rho u'v'}) = -\overline{\rho q'v'} + f\partial_z\left(\rho\frac{\overline{\theta'v'}}{S}\right). \tag{2.10}$$

Because both potential vorticity and heat are conserved following particle trajectories, Green (1970) argues that potential vorticity is "diffused" by baroclinic eddies down the mean gradients with the same "diffusivity" of the heat flux, i.e.

$$\overline{q'v'} = -\kappa\partial_y\overline{q}, \tag{2.11}$$

where κ is given in (2.5).

If $\overline{u}$ denotes the zonally averaged flow, the zonally averaged potential vorticity is

$$\overline{q} = \beta y - \overline{u}_y + f\rho^{-1}\partial_z(\rho\overline{\theta}/S). \tag{2.12}$$

Using (2.10) through (2.12) and the parametrization (2.4), the divergence of the zonally averaged momentum becomes

$$\partial_y(\overline{u'v'}) = \kappa(\beta - \overline{u}_{yy}) - \partial_z\kappa(f/S)\partial_y\overline{\theta}. \tag{2.13}$$

Given the vertical distribution of temperature, (2.6), and the thermal wind balance, $\overline{u}$ is given by

$$\overline{u} = \overline{u}_s(y,t) - (g/f\Theta)z\partial_y\theta_s(y,t), \tag{2.14}$$

where Θ is the constant temperature (in Kelvin) around which the Boussinesq approximation is pivoted. $\overline{u}_s$ is the surface wind, related to the surface stress by the linearized drag-law

$$\tau = \rho_s\gamma\overline{u}. \tag{2.15}$$

With this final parametrization, the surface stress satisfies

$$\tau - d_e \kappa_s \gamma^{-1} {\partial_y}^2 \tau = -\rho_s \kappa_s d_e d^{-1} \left[\beta d + \frac{f}{S} \left(\partial_y \theta_s + L_\rho^2 {\partial_y}^3 \theta_s \right) \right], \tag{2.16}$$

subject to the boundary conditions, $\tau = 0$ at the meridional boundaries of the domain $y = 0, L_y$. In (2.16) L_ρ, defined as

$$L_\rho \equiv [d d_e g S/(f^2 \Theta)]^{1/2}, \tag{2.17}$$

is the baroclinic deformation radius of the atmosphere. Green's parametrization (2.16) thus relates the wind-stress to gradients in the zonally and vertically averaged potential temperature.

The requirement of no-net torque of the atmosphere on the earth's surface is also imposed:

$$\int_0^{L_y} \tau \, \mathrm{d}y = 0. \tag{2.18}$$

This additional constraint can be satisfied because the vertical scale of the eddy flux, d, is considered an unknown, and it is determined as part of the solution. In the application to a climate problem, we follow the advice of White and Green (1984) that global conservation laws should be given priority over the local spatial dependence suggested by instability analysis when constraining the eddy-transfer parametrizations.

Because the high order derivatives in (2.16) are small except in boundary layers, the no-net stress constraint gives

$$d \approx \frac{f[\theta_s(0) - \theta_s(L_y)]}{\beta S L_y}. \tag{2.19}$$

In this way the vertical scale height of the eddy flux, d, decreases with increasing stratification or β, and increases with the meridionally averaged mean potential temperature gradient.

The approximate expression (2.19) shows that d is the latitudinal average of the parameter, h, defined as

$$h \equiv f |\partial_y \theta| (\beta S)^{-1}, \tag{2.20}$$

and introduced by Charney (1947) as a local measure of the vertical scale of baroclinic eddies (see also Held 1978). Thus, in our simplified model, the scale height of the baroclinic eddies, determined by the global momentum constraint, is proportional to the *averaged* Charney's scale height, rather than the *local* scale height as in Branscome (1983).

c. Summary

Using arguments based on conservation of heat and momentum, it is possible to parametrize the heat and momentum flux provided by baroclinic eddies in terms of the longitudinally averaged surface atmospheric temperature. This leads to two diagnostic equations, (2.7) and (2.16), relating the zonally averaged surface air temperature, θ_s, the zonally averaged wind-stress, τ, and the sea surface temperature, T_s. Although crude, the parametrizations used here guarantee global conservation of heat and momentum, which are essential constraints in climate dynamics.

3. The oceanic budget

In order to complete the heat budget for the atmosphere, it is necessary to determine the sea surface temperature. This is done by considering the heat balance in the ocean: here we ignore the contribution to the heat budget due to the thermohaline overturn, and assume that the water below the thermocline is at rest. In this way, the oceanic heat transport is due only to the wind-driven circulation.

a. The mechanical balance

The simplest model for wind-driven currents considers flow vertically averaged from the bottom of the thermocline, at $z = -H$, to the ocean's surface. The vertically integrated horizontal velocity is entirely determined by the curl of the wind stress. Here, we restrict our attention to quasi-geostrophic dynamics, with the velocity determined by the transport streamfunction, through the relation

$$\left(\int_{-H}^{0} u \,\mathrm{d}z, \int_{-H}^{0} v \,\mathrm{d}z\right) = (-\psi_y, \psi_x). \tag{3.1}$$

The evolution of ψ is governed by the large-scale limit of the equivalent barotropic vorticity equation:

$$\psi_t - c\psi_x = A_h \nabla^2 \psi + R^2 \rho_w^{-1} \partial_y \tau. \tag{3.2}$$

Here $c \equiv \beta R^2$ is the speed of the long Rossby waves and R is the baroclinic deformation radius: the relative vorticity terms have been ignored because they are small for large scale flow. Moreover, with relative vorticity the equivalent barotropic equation exhibits intrinsic low-frequency time-dependence even for prescribed and steady wind stress (Berloff and Meacham 1997, McCalpin and Heidvogel 1996). Because here the focus is on coupled dynamics, the sources of variability of the uncoupled problems are purposefully suppressed.

Dissipation is in the form of downgradient potential vorticity diffusion with a diffusivity, A_h, appropriate for mesoscale flows. With this crude parametrization of oceanic baroclinic eddies the condition of no-flow across the domain boundaries can be enforced. In practice, to properly resolve the western boundary layer, of width A_h/c, the eddy-diffusivity in the $x-$*direction* is set to be larger by a factor of 10 than the diffusivity in the $y-$*direction*. In other words, the downgradient diffusion for both temperature and vorticity is anisotropic. We have repeated the calculation presented in section 6 with twice as much resolution and half the viscosity in the x-direction (so that the ratio of the eddy-diffusivity in x to the eddy-diffusivity in y is reduced to five), and have found small quantitative changes and no qualitative changes.

Consistently with the quasi-geostrophic approximation, H, β and R are all constant.

b. The ocean heat balance

In the spirit of Behringer et al. (1979) we consider the oceanic heat budget vertically integrated from the ocean surface down to the level where the wind-driven circulation becomes negligible, $z = -H$. Because only the vertically integrated currents are calculated in the oceanic momentum budget, only the vertically averaged temperature contributes to the oceanic heat budget. In other words, we neglect the contribution to the vertically averaged heat transport due to the correlation between the velocity and the temperature that depart from the vertical average. In this way, the upper ocean heat content is directly proportional to the SST, T_s, which evolves according to

$$c_w\rho_w\left[H\partial_t T_s - \partial_x\left(T_s\psi_y\right) + \partial_y\left(T_s\psi_x\right)\right] = F_0 + c_w\rho_w A_h H\nabla^2 T_s. \tag{3.3}$$

Here we have assumed that the heat flux across the bottom of the wind-driven bowl is negligible and that the small scale processes can be parametrized as down-gradient diffusion. At the solid boundaries, no flux conditions are imposed. The heat flux at the ocean's surface, F_0, is equal to that at the bottom of the atmosphere, so that global heat balance is enforced. See (2.3) for the expression of F_0.

c. Summary

With the specification of the radiative fluxes at the top of the ocean, $\mathcal{F}(y)$, and at the top of the atmosphere, Q_i, the set (2.7), (2.16), (3.2) and (3.3) is a closed system in the two atmospheric variables, θ_s and τ, and the two oceanic variables, T_s and ψ. The atmospheric variables are diagnostic, because on the time scale of oceanic motion, the atmosphere adjusts "instantaneously". The oceanic variables are prognostic and set the time scales of evolution in the coupled-system.

4. Geometry, forcing and parameters

The eddy parametrization of Green (1970) can be generalized to a spherical geometry, without abandoning the quasi-geostrophic approximation (White 1977). Nevertheless, given the many crude simplifications made here, a cartesian geometry is retained although a whole hemisphere is considered. On a β-plane, it is not obvious which is the most appropriate latitudinal extent of an hemisphere. Here, L_y is identified with the pole-to-equator distance on the sphere.

For the ocean, a single rectangular basin is considered, bounded to the north and south by the pole and the equator respectively, that is by the atmosphere's meridional boundaries. The longitudinal width of the basin is denoted by L_x and is a fraction, r, of the hemispherical extent.

a. The specification of the radiative forcing

The net short wave radiation at the top of the atmosphere, $Q_i(y)$, is approximated with a simple curve that fits the Northern hemisphere data published in Stephens et al. (1981). Specifically we set

$$Q_i = -Q_1 \sin^2\phi + Q_2 \sin\phi + Q_3, \tag{4.1}$$

with the latitude, ϕ, and the β-plane coordinate, y, connected by

$$y = L_y \sin\phi. \tag{4.2}$$

The coefficients of the polynomial for Q_i are given by

$$Q_1 = 322.72, \quad Q_2 = 75.26, \quad Q_3 = 309.40, \tag{4.3}$$

all values in (4.3) are in $\mathrm{W\ m^{-2}}$.

The heat flux that enters the ocean in thermal equilibrium with the atmosphere, $\mathcal{F}$, is expressed as a polynomial of the form:

$$\mathcal{F} = p\left(F_1 \sin^4\phi + F_2 \sin^3\phi + F_3 \sin^2\phi + F_4 \sin\phi + F_5\right). \tag{4.4}$$

The coefficients, F_i, of the polynomial for $\mathcal{F}$ are obtained by fitting the results of Haney (1971), and setting the constant p to unity. In this case we obtain

$$F_1 = 511.6, \quad F_2 = -1,306.9, \quad F_3 = 1,233.3, \quad F_4 = -569.9, \quad F_5 = 131.7, \tag{4.5}$$

all in units of $\mathrm{W\ m^{-2}}$. However, the errors involved in the estimate of $\mathcal{F}$ from data are very large, so we introduce a constant, p, with values between zero and unity, that allows us to rescale the amplitude of the imposed flux. Figure 1 shows Q_i and $\mathcal{F}$ as a function of y, for $p = 1/2$, the value used in all the calculations presented. $\mathcal{F}$ is rather small outside the equatorial region, and has thus little influence in mid-latitudes, where the formulation of the coupled dynamics proposed here is most appropriate. To be sure, we have repeated the calculations of sections 5 and 6 with $p = 0$ and $p = 1$ and only small quantitative changes confined to the low latitudes were found.

b. A choice of parameters

Besides the geometry of the model atmosphere and ocean, and the prescription of the imposed fluxes at the top of the atmosphere and ocean, the numerical value of many parameters must be specified. Although a thorough exploration of the parameter space is not feasible, the relative simplicity of the present formulation allows to examine the dependence of the solutions on a subset of parameters, especially those associated with poorly understood sub-grid parametrizations.

We begin with the least controversial and most uncritical choices for the atmospheric portion of the model. With the β-plane centered at 45 °N we set:

$$\begin{aligned} f &= 1 \times 10^{-4}\ \mathrm{s}^{-1} & \rho_s &= 1.25\ \mathrm{kg\ m}^{-3} \\ L_y &= 1 \times 10^{7}\ \mathrm{m} & S &= 5 \times 10^{-3}\ {}^\circ\mathrm{C\ m}^{-1} \\ \beta &= 1.6 \times 10^{-11}\ \mathrm{m}^{-1}\ \mathrm{s}^{-1} & \Theta &= 273\ \ {}^\circ\mathrm{K} \\ D &= 8 \times 10^{3}\ \mathrm{m} & g &= 9.8\ \mathrm{m\ s}^{-2}. \\ c_{pa} &= 1000\ \ \mathrm{J}\ {}^\circ\mathrm{C}^{-1}\ \mathrm{kg}^{-1} \end{aligned} \tag{4.6}$$

The constants A and B entering the long-wave radiation parametrizations are chosen so that the averaged surface temperature matches the observed value in the Northern hemisphere, i.e. 16 °C, and so that the pole to equator temperature difference in radiative equilibrium, i.e. with neither eddies nor ocean flow, is 100°C. Given the expression for Q_i, these constraints lead to

$$A = 200\ \mathrm{W\ m}^{-2} \qquad B = 2.475\ \mathrm{W\ m}^{-2}\ {}^\circ\mathrm{C}^{-1}. \tag{4.7}$$

Two more parameters pertaining to the atmospheric dynamics must be specified: the amplitude of the baroclinic eddies diffusivity, κ_s, and the surface drag coefficent, γ, which are both taken as constants. This choice might seem unsatisfactory, especially for γ, which is typically observed to be proportional to the surface wind speed. However, because the relation between the stress and the surface velocity is nonlinear, it is not clear that including the dependence on the *zonally averaged* wind is preferable than taking γ constant. White

(1977) discusses the relative merit of the two options and concludes that "the detailed form of the stress law is not a critical factor in determining the solution $\tau(y)$". This insensitivity is not surprising because the drag coefficent only affects τ through a small curvature term [the second term on the left hand side of (2.16)]. We thus set:

$$\gamma = 2.4 \times 10^{-2} \text{ m s}^{-1}. \tag{4.8}$$

The amplitude of the eddy diffusivity, κ_s, is a crucial parameter because the momentum flux convergence, and thus the wind-stress, are directly proportional to κ_s. At any rate, a limited exploration of the solutions' behavior as a function of κ_s is presented in sections 5 and 6. For the calculation presented in section 5 we chose:

$$\kappa_s = 3 \times 10^6 \text{ m}^2 \text{ s}^{-1}. \tag{4.9}$$

The parameters for the single ocean basin are chosen to approximate the North Pacific at 45 °N, we thus set:

$$\begin{aligned} L_x &= 0.825 \times 10^7 \text{ m} & c_w &= 4000 \ \text{ J °C}^{-1} \text{ kg}^{-1} \\ r &= 0.3 & \rho_w &= 1000 \text{ kg m}^{-3} \\ H &= 1 \times 10^3 \text{ m} & R &= 3.5 \times 10^4 \text{ m.} \end{aligned} \tag{4.10}$$

The thermal exchange coefficent, λ, is taken to be constant, with a value at the low end of the range estimated by Haney (1971). The coefficient of eddy-diffusion, A_h, has been estimated by direct measurements to be of the order of 500 $\text{m}^2 \text{ s}^{-1}$ in areas of moderate mesoscale activity. Our reference values are

$$\lambda = 23 \ \text{ W m}^{-2} \text{ °C}^{-1} \qquad A_h = 200 \text{ m}^2 \text{ s}^{-1}. \tag{4.11}$$

5. A steady solution

The solution for the set of parameters quoted in the previous section is now discussed. This solution is obtained solving the system (2.7), (2.16), (3.2) and (3.3) numerically. For this set of parameters the solution reaches a steady state which, insofar as we could test, is independent of the initial condition. Figure 2 shows τ on the left panel and the streamfunction transport on the right panel. Because on the $\beta-$plane the equatorial easterlies are exaggerated, the cyclonic tropical gyre is very vigorous, while the midlatitude values of τ are close to those observed in the present climate. At any rate, taking into account the obvious deficencies due to the geometry of the model, the wind-stress distribution produces a qualitatively correct circulation pattern.

The surface ocean temperature, T_s, is shown in figure 3 on the right panel. The forcing comes from the zonally averaged surface air temperature, θ_s, which is shown on the left panel of the same figure. Because the interaction with the zonally averaged atmosphere forces temperature variations that are independent of longitude, departures from zonality are confined to the western side of the basin, where the advection by ocean currents is strongest. However, the region of substantial longitudinal modulation in the ocean surface temperature is not confined to the western boundary current: the temperature western boundary layer is much wider than the transport boundary layer (cf. figure 2 and figure 3). The main effect of advection is the formation of a strong thermal front at the boundary of the subtropical and subpolar gyres, below the maximum of the westerlies. In this region, the heat flux at the air-sea boundary, F_0, contoured in figure 4, reaches its extreme values. The northward advection on the western side of the subtropical gyre produces a wide region of large heat loss to the atmosphere, while on the subpolar side there is a smaller heat gain. Both features are western intensified and in qualitative agreement with the observed annual average published in Moisan and Niiler (1998). However, the ocean heat gain in the subpolar gyre is much larger than that estimated through observations, presumably because of the unrealistic northern extent of the model basin which results in the southward advection of very low oceanic temperatures.

Naturally the heating and cooling dipole below the westerly region contributes to the reshaping of the atmospheric temperature gradient. Specifically, in steady state the zonally averaged ocean heat budget is, from (3.3):

$$c_w \rho_w \partial_y \left(\overline{T_s \psi_x} - A_h H \partial_y \overline{T_s} \right) = \overline{F_0}, \tag{5.1}$$

where the left hand side is the divergence of the zonally averaged ocean heat transport. Applying this identity to the atmospheric heat budget (2.7), we obtain, after a simple integration in latitude, the global heat budget:

$$-c_{pa} \rho_s \kappa_s d_e \partial_y \theta_s + r c_w \rho_w \left(\overline{T_s \psi_x} - A_h H \partial_y \overline{T_s} \right) = \int_0^y (Q_i - B\theta_s - A) \, \mathrm{d}\tilde{y}. \tag{5.2}$$

By construction, global conservation of heat is enforced and thus, in steady state, the sum of the atmosphere's northward heat transport [the first term on the left hand side of (5.2), denoted with ANHT henceforth] and the ocean's northward heat transport [the second term on the left hand side of (5.2), denoted with ONHT henceforth] at any given latitude is balanced by the integral of the net heat flux from the equator to that latitude [the left hand side of (5.2)]. The latter is the residual between the incoming short wave radiation and the outgoing long wave radiation.

Figure 5 shows the radiative equilibrium temperature and θ_s. The difference between these two fields is proportional to the heating rate of the planet. For reference, the atmospheric surface temperature if there were no ocean is also plotted. The latter is obtained by setting $r = 0$ in (2.7). Because the ocean heat transport is everywhere northward, it reduces the equator to pole temperature difference by about 3 °C, but, as apparent later, it does not reduce the atmospheric temperature gradient everywhere. The neglect of the mean ageostrophic Hadley circulation and of oceanic upwelling results in large surface temperature in the tropics: this is to be expected in a dry model, with a parametrization of the eddies appropriate for midlatitudes.

Figure 6 shows the northward heat fluxes as a function of latitude, both with and without ocean (dashed-dotted line). Firstly, the total northward heat flux is larger when the effect of the ocean is included (solid line). This is because the ONHT reduces the equatorial temperatures (cf. figure 5) and the outgoing radiation. Therefore, the earth receives more heat in low latitudes. The difference between the two total northward heat fluxes is greatest at the peak of the ONHT, which coincides with the latitude at which θ_s with and without ocean are equal.

The other important effect of the ONHT (dotted line in figure 6) is to modulate the ANHT (dashed line): at the maxima of ONHT, located at the gyre transport maxima, the ANHT is substantially less than the value obtained without ocean (dashed-dotted line). At the confluence of the subtropical and subpolar gyres, where the oceanic heat transport reaches a local minimum, the burden of balancing the incoming net heat is carried almost entirely by the atmosphere, so the ANHT is maximum. The net result of the ocean's contribution to the heat budget is a sharpening of the ANHT maximum at the boundary between the subpolar and subtropical gyres. Because the ANHT is proportional to the gradient of the potential temperature, this peak coincides with a maximum in baroclinicity. In this sense, we reach the same conclusion of Hoskins and Valdes (1990): the ocean's heat flux is a determining factor in the maintenance of the mean position of the baroclinic wave-guide in the midlatitude atmosphere. At least in the context of this minimal model, the coincidence of the large surface heat flux dipole shown in figure 4 with the storm-track position is part of a global heat balance requirement.

A complementary interpretation of the interaction between the oceanic gyres and the wind-stress is that there is a positive feedback between these two components. Suppose that there is a perturbation that accelerates the westerlies' maximum. In order to conserve the net torque such a perturbation must be accompanied by an acceleration of the easterlies elsewhere in the domain. In this way the curl of the wind-stress is locally increased and both the subtropical and the subpolar gyres are spun up. The increased oceanic transport sharpens the oceanic thermal front under the maximum of the westerlies, i.e. at the midlatitude intergyre boundary. Increased oceanic thermal gradients enhance the atmospheric temperature gradient, accelerating further the surface westerlies maximum.

This sharpening process is arrested on the scale of the baroclinic deformation radius of the atmosphere, L_ρ, by the flux of relative vorticity [the second term on the right hand side of (2.16)], which diffuses momentum down the mean gradient, and thus acts to decelerate the westerlies.

Notice that the sharpening of the mean atmospheric thermal gradients by oceanic processes emerges even in a zonally averaged atmosphere, where the land-ocean thermal contrast is unresolved. Presumably the ocean also modulates the longitudinal distribution of atmospheric mean thermal gradients and thus regulates the zonal localization of baroclinic wave growth in the atmosphere.

6. A decadal oscillation

The approach to the steady solution discussed in the previous section from arbitrary initial condition is through a damped oscillation. In this section we show that a small change in the choice of parameters leads to sustained oscillations. Specifically, the atmospheric eddy diffusivity is decreased by 10% to yield:

$$\kappa_s = 2.7 \times 10^6 \ \mathrm{m}^2 \ \mathrm{s}^{-1}. \tag{6.1}$$

This change leads to a destabilization of the steady equilibrium illustrated in the previous section and the emergence of a sustained oscillation through a Hopf bifurcation.

The oscillation is characterized by time dependence in all fields, as exemplified in Figure 7, which shows τ as a function of latitude and time after the system equilibrates into a periodic solution, with period 17.7 years, independent of the initial condition. Southward migrating disturbances periodically displace the maximum of the westerlies. The decadal variability is confined to the midlatitudes, on the northern side of the subtropical gyre.

The time-averaged fields differ little from the steady state found in the previous section except for some quantitative differences highlighted in the following.

a. Climatology

The wind stress and streamfunction, averaged over one period, are shown in figure 8. Comparison with figure 2 illustrates that the time-averaged wind-stress maximum is about 6% smaller than the steady solution obtained for a larger eddy diffusivity. This decreased wind-stress results in an oceanic flow which is slightly weaker than that shown in figure 2. However, there are no qualitative differences between the fields in figures 2 and 8.

The atmospheric and oceanic temperature, averaged over one period of the oscillation, are shown in figure 9. The time-averaged thermal front under the westerlies' maximum is less pronounced than that of the steady solution shown in figure 2. The weakened thermal gradient is due to two effects: firstly, the oceanic circulation is weaker and thus the confluence of southerly warm water and northerly cold water at the intergyre boundary is less. Secondly, because the actual solution is time-dependent, and the maximum of the westerlies periodically migrates meridionally, as shown in figure 7, there is a small time-averaged temperature exchange at the intergyre boundary. Indeed, the associated unstable steady solution (not shown here) has a sharper temperature gradient under the westerlies' maximum than the time-averaged solution. Nevertheless, the time-mean heat flux at the air-sea interface is almost identical to that of figure 4.

The time averaged northward heat fluxes, shown in figure 10, display the same qualitative features obtained for a larger eddy diffusivity, except that the maxima in both the ONHT and the ANHT are decreased, as expected with smaller wind-stress and a diminished eddy diffusivity for the atmosphere. However, both the position and the width of the baroclinic wave-guide are the same in figure 6 and 10.

b. Variability

Three equally spaced snapshots of the transport streamfunction, superimposed on deviations of T_s from the time mean during one period of the oscillations are shown in figure 11. A sequence of positive and negative T_s anomalies are generated at the western confluence of the subpolar and subtropical gyre, where the mean thermal front is sharpest. Subsequent to their generation the T_s anomalies propagates southwards and clockwise until they are "absorbed" at the western boundary. Although the period is 17.7 years, each individual anomaly takes roughly two periods, or 35 years, to make the complete circuit around the subtropical gyre, from the generation site at 40°N to the absorption site at 20°N. For example, the positive T_s anomaly located at 40°N at year 0 can be followed southwards in years 6.2 and 11.9 until, at year 17.7 (one period), it reaches 30°N. Subsequently this warm anomaly is compressed as it moves south and west, and reaches the western boundary at 20°N at year 35.4.

While advected around the gyre, T_s anomalies are continuously relaxed towards the zonally averaged surface air temperature. This process redistributes the ocean heat zonally, accounting for the longitudinal elongation of the anomalies as they travel southward. At the same time, the exchange with the atmosphere damps the temperature anomalies, so that their amplitude decreases during the propagation away from the generation site at the gyres' boundary.

The fluctuations in T_s are accompanied by anomalies in θ_s which are substantially weaker (the departures of θ_s from the time mean are a factor of ten smaller than the fluctuations in $\overline{T_s}$). However, these weak potential temperature changes induce sizeable fluctuations in the wind-stress (cf. figure 7) which lead to substantial modulation in ψ, as can be seen in figure 11. Without inertia and solely caused by the wind-stress, the subtropical gyre displays a time-dependent recirculation-like feature, which periodically shifts the maximum transport meridionally. This result supports the hypothesis of Behringer et al. (1979) that thermal feedback between ocean and atmosphere produces a wind-stress pattern which promotes the formation of recirculation.

The wind-driven currents adjust to changes in the wind-stress with a delay, t_0, due to the transit time of westward propagating baroclinic Rossby waves. The delay is given by

$$t_0 \equiv \frac{L_x - x}{\beta R^2}, \tag{6.2}$$

so it vanishes on the eastern boundary and reaches its maximum of 13.3 years on the western boundary. Because the oceanic heat transport is maximum at the seaward edge of the western boundary current, where the delay is longest, changes in oceanic northward heat flux are not concurrent with changes in atmospheric heat flux, and the solution which satisfies the global heat balance is oscillatory in time, rather than steady.

Figure 12a shows the oscillation period as a function of the delay at the western boundary, $L_x/(\beta R^2)$. The delay is varied by changing the Rossby deformation radius, R. Firstly, sustained oscillations are only obtained for an intermediate range of delays. Secondly, the period is not linearly proportional to the Rossby wave delay, but scales as the square root of t_0. This indicates that another timescale is involved in the period of the oscillation. In figure 12b the oscillation period is plotted as a function of the advective time scale around the subtropical gyre, measured here by $L_x L_y H/\psi_{max}$. The advective time scale is varied, keeping everything else constant, by artificially increasing the amplitude of the wind-stress, τ. In summary the period of the oscillatory solution scales as the geometric mean of *two* time-scales: the Rossby wave delay and the advection time around the gyre. However, the Rossby wave delay is essential for oscillatory behaviour. Another calculation, not shown here, with parameters identical to those of figure 12a except that the Rossby wave speed is infinite, reaches a steady state without any indication of damped oscillations.

c. Heat-fluxes

The time-dependent anomalies in the ψ and T_s field lead to substantial fluctuations in the ocean northward heat flux (ONHT), accompanied by out of phase fluctuations in the ANHT. In a time-dependent equilibrium, the total heat budget is given by

$$\mathrm{ANHT} + \mathrm{ONHT} + r c_w \rho_w H \int_0^y \partial_t \overline{T_s}\ \mathrm{d}\tilde{y} = \int_0^y (Q_i - B\theta_s - A)\ \mathrm{d}\tilde{y}. \qquad (6.3)$$

Because the fluctuations in time of the outgoing long wave radiation are negligible compared to those of the heat transport terms, to a good approximation the right hand side of (6.3) can be considered in steady state. However, the oceanic heat storage rate [the third term on the left hand side of (6.3)] contributes as much as the ANHT to the time-dependence of the global heat budget. Figure 13 shows the heat transports anomalies and the heat storage rate at $y = 5000$ km, during one period of the oscillation: all three terms are important in different phases of the oscillation. Specifically, fluctuations in the oceanic component of the heat transport lead changes in the atmospheric flux by about 6 years, which is approximately one third of the oscillation period. The essential point is that the ONHT and the ANHT are out of phase: this is the hallmark of a genuinely coupled oscillation, where neither the atmosphere is passively responding to the ocean intrinsic time-dependence nor the ocean is driven by the atmosphere's natural low-frequency variability. As originally postulated by Bjerknes (1964) fluctuations in the wind-driven currents lead to heat flux fluctuations in the atmosphere that are accompanied by changes in the potential temperature gradients and thus in the wind that drives the ocean flow.

7. Summary and conclusions

By coupling two basic models of the midlatitude circulation of the atmosphere and of the ocean through the thermal heat balance, a possible interaction between the wind and the ocean gyres has been isolated. Although the separate modules are highly simplified and parametrized, global conservation of heat and momentum is enforced.

We have demonstrated that the large dipole of air-sea heat exchange at the boundary between the subtropical and subpolar gyre narrows and amplifies the atmospheric storm-track. At this location an acceleration of the westerlies spins up the gyres thus sharpening the oceanic thermal front. This leads to an increased thermal gradient in the atmosphere, which further accelerates the westerlies on scales larger than the atmosphere's deformation radius, and decelerates the westerlies on smaller scales. A complementary interpretation is that the oceanic northward heat transport modulates the atmospheric northward heat transport. Because the adjustment of oceanic heat transport to changes in the winds is delayed by the slow propagation of baroclinic Rossby waves, the global heat balance is achieved through a solution that is periodic in time rather than steady. The period of the oscillations is proportional to the geometric mean of the Rossby wave delay and the gyral advection time-scale.

The coupling between the atmosphere and the ocean is most effective at the thermal front located at the midlatitude intergyre boundary. At this location small changes in the wind-driven flow produce large heat flux anomalies. Once the anomalies are generated, they travel clockwise around the subtropical gyre as they slowly decay. The advection of thermal disturbances from the midlatitude to the tropics has been documented in the North Pacific (Schneider et al. 1999 and Zhang et al. 1998) and might be responsible for the decadal modulation of tropical dynamics.

Unfortunately, the coupled modes of variability documented here are at the location where the separate oceanic and atmospheric system have maxima of intrinsic variability (purposefully suppressed in the present model). This indicates that separating coupled from intrinsic variability might be difficult in the analysis of natural data or of simulata from eddy resolving coupled general circulation models.

The hallmark of coupled oscillations in our model is that anomalies in the atmospheric and oceanic northward heat transports are of comparable amplitude and out of phase. Specifically, changes in the oceanic heat transport lead fluctuations in the atmospheric transport by about six years, i.e. approximately one third of the oscillation period. If this phase relation survives when other sources of variability, neglected in the present formulation, are included then enhanced predictability of decadal shifts in midlatitude weather patterns can result from the oceanic modulation of the global heat budget.

Acknowledgements

Numerous conversations with Bill Young are gratefully acknowledged. Funding for this research is provided by the National Science Foundation and the Department of Energy.

References

Anderson, D.L.T., A.E. Gill, 1975: Spin-up of a stratified ocean, with applications to upwelling. *Deep-Sea Res.*, **22**, 583-596.

Behringer D., Regier L., Stommel H., 1979: Thermal feedback on wind-stress as a contributing cause of the Gulf Stream. *J. Marine Res.*, **37**, 699-709

Berloff P. and Meacham S., 1997: The dynamics of an equivalent-barotropic model of the wind-driven circulation. *J. Mar. Res.*, **55**, 407-451.

Bjerknes, J., 1964: Atlantic air-sea interaction. *Advances in Geophys.*, **10**, 1-82.

Branscome, L.E., 1983: A parameterization of transient eddy heat flux on a beta-plane. *J. Atmos. Sci.*, **40**, 2508-2521.

Bryden, H.L., D.H. Roemmich, J.A. Church, 1991: Ocean heat transport across 24 degrees N in the Pacific. *Deep-Sea Res. A*, **38**, 297-324.

Charney, J.G., 1947: The dynamics of long waves in a baroclinic westerly current. *J. Meteor.*, **4**, 135-163.

Ferranti, L., F. Molteni and T.N. Palmer, 1994. Impact of localized tropical and extratropical SST anomalies in ensamble of seasonal GCM integrations. *Quart. J. R. Met. Soc.*, **120**, 1613-1645.

Green, J.S.A., 1970: Transfer properties of the large scale eddies and the general circulation of the atmosphere. *Quart. J. R. Met. Soc.*, **96**, 157-185.

Haney, R.L., 1971: Surface thermal boundary condition for ocean circulation models. *J. Phys. Oceanogr.*, **1**, 241-248.

Held, I.M., 1978: The vertical scale of an unstable baroclinic wave and its importance for eddy heat flux parametrizations. *J. Atmos. Sci.*, **35**, 572-576.

Hoskins, B.J. and P.J. Valdes, 1990: On the existence of storm-tracks. *J. Atmos. Sci.*, **47**, 1854-1864.

Kushnir, Y. and I. Held, 1996. Equilibrium atmospheric response to North Atlantic SST anomalies. *J. Climate*, **7**, 141-157.

Macdonald, A.M. and C. Wunsch, 1996: An estimate of global ocean circulation and heat fluxes. *Nature*, **382**, 436-439.

McCalpin, J. and Haidvogel D., 1996. Phenomenology of the low-frequency variability in a reduced-gravity, quasigeostrophic double-gyre model. *J. Phys. Oceanogr.*, **26**, 739-752.

Moisan, J.R. and P.P. Niiler, 1998: The seasonal heat budget of the North Pacific: Net heat flux and heat storage rates (1950-1990) *J. Phys. Oceanogr.*, **28**,401-421.

Palmer, T.N. and Sun Z., 1985. A modelling and observational study of the relationship between sea surface temperature in the north-west Atlantic and the atmospheric general circulation. *Quart. J. R. Met. Soc.*, **111**, 947-975.

Peng, S., L.A. Mysak, H. Ritchie, J. Derome and B. Dugas, 1995: The difference between early and middle winter atmospheric response to sea surface temperature anomalies on the January climate of a general circulation model. *J. Climate*, **8**, 137-157.

Pitcher, E.J., M.L. Blackmon, G.T. Bates and S. Munos, 1988: The effect of North Pacific sea surface temperature anomalies on the January climate of a general circulation model. *J. Atmos. Sci.*, **45**, 172-188.

Schneider N., Miller, A.J., Alexander, M.A. and Deser, C., 1999: Subduction of decadal North Pacific temperature anomalies: observations and dynamics. *J. Phys. Oceanogr.*, in press.

Stephens, G.L., G.G. Campbell and T.H. Vonder Haar, 1981: Earth radiation budgets. *J. Geophys. Res.*, **86**, 9739-9760.

Stommel, H., 1948: The westward intensification of wind-driven ocean currents. *Trans. Amer. Geophys. Union*, **29**, 202-206.

Stone, P.H. and M.-S. Yao, 1987: Development of a two-dimensional zonally averaged statistical-dynamical model. Part II: the role of eddy momentum fluxes in the general circulation and their parametrization. *J. Atmos. Sci.*, **44**, 3769-3786.

Stone, P.H. and M.-S. Yao, 1990: Development of a two-dimensional zonally averaged statistical-dynamical model. Part III: the parametrization of eddy fluxes of heat and moisture. *J. Climate*, **3**, 726-740.

Trenberth, K.E. and A. Solomon, 1994: The global heat balance: heat transports in the atmosphere and ocean. *Clim. Dyn.*, **10**, 107-134.

Veronis, G. and H. Stommel, 1956: The action of variable wind stresses on a stratified ocean, *J. Mar. Res.*, **15**, 43-75.

White, A.A., 1977: The surface flow in a statistical climate model - a test of a parameterization of large-scale momentum fluxes. *Quart. J. R. Met. Soc.*, **103**, 93-119.

White, A.A. and J.S.A. Green, 1984: Transfer coefficient eddy flux parameterizations in a simple model of the zonal average atmospheric circulation. *Quart. J. R. Met. Soc.*, **110**, 1035-1052.

Zhang, R-H. Rothstein, L.M. and Busalacchi, A.J., 1998: Origin of upper-ocean warming and El Niño change on decadal scales in the tropical Pacific Ocean. *Nature* **391**, 879-883 (1998).

Figure and Table Captions

Figure 1. The incoming radiation at the top of the atmosphere, Q_i, and the heat flux at the top of the ocean, $\mathcal{F}$, when $T_s = \theta_s$, both as a function of latitude. The units are Wm^{-2}.

Figure 2. The zonally averaged wind-stress and surface winds are shown on the left panel: the westerlies reach a maximum of $3.2\mathrm{ms}^{-1}$, leading to a maximum eastward stress of $0.097\mathrm{Nm}^{-2}$. The equatorial easterlies peak at $-3.7\mathrm{ms}^{-1}$, leading to a maximum westward stress of $-0.112\mathrm{Nm}^{-2}$. The right panel shows the corresponding transport streamfunction in sverdrups (1 sverdrup=$10^6\mathrm{m}^3\mathrm{s}^{-1}$) and the contour interval is 5 sverdrups. For reference, the latitudinal coordinate is given both in units of distance (left) and in degrees on the right. The values for all parameters are given in section 4.

Figure 3. The zonally averaged surface air temperature, graphed on the left panel, forces latitudinal gradients in the sea surface temperature, contoured in the right panel. The advection by the ocean flow, shown in figure 2, creates longitudinal gradients in T_s. Because of the intensitity of the tropical gyre, T_s is homogenized in that region. The units are in °C.

Figure 4. The surface heat flux, proportional to the difference of the two fields shown in figure 3, reaches a minimum of $-440\mathrm{Wm}^{-2}$ at the northern edge of the subtropical gyre and a maximum of $300\mathrm{Wm}^{-2}$ at the southern edge of the subpolar gyre.

Figure 5. The zonally averaged surface air temperature in the presence of both atmosphere and ocean heat transport (solid line), with atmospheric transport only (dashed line), and without any transport (dashed-dotted line). The units are in °C.

Figure 6. The zonally averaged northward heat fluxes in Watts. The ocean northward heat flux (dotted line) is everywhere positive and has maxima at the peak of the ocean gyres' transport. At the maxima of ONHT the atmospheric flux (dashed line) is reduced leading to a peak under the westerlies' maximum which is sharper than that obtained if there were no ocean (dashed-dotted line). The total northward heat flux (solid line) with ocean flow included (solid line) exceeds the heat transport without any ocean flow (dashed-dotted line).

Figure 7. τ as a function of time and latitude. The wind-stress is periodic in time with a period of 17.7 years. The units are Nm^{-2}, the contour interval is $0.02\mathrm{Nm}^{-2}$ and negative values are dashed. All parameters are as in section 4 except that the eddy diffusivity is reduced by 10%.

Figure 8. The time averaged wind-stress and surface winds are shown on the left panel: the westerlies reach a maximum of $3.0\mathrm{ms}^{-1}$, leading to a maximum eastward stress of $0.091\mathrm{Nm}^{-2}$. The equatorial easterlies reach $-3.5\mathrm{ms}^{-1}$, leading to a maximum westward stress of $-0.1\mathrm{Nm}^{-2}$. The right panel shows the corresponding time averaged transport streamfunction in sverdrups.

Figure 9. The time averaged surface air temperature is graphed on the left panel, and the time averaged sea surface temperature is contoured in the right panel. Because of the weaker oceanic circulation the SST front at the midlatitude intergyre boundary is less sharp than that shown in figure 3. The units are in °C.

Figure 10. The time-averaged northward heat fluxes in Watts. The maxima of both ocean northward heat flux (dotted line) and atmospheric northward heat transport (dashed line) are smaller than for those obtained in figure 6, leading to a reduced total northward heat flux both with (solid line) and without (dashed-dotted line) ocean compared to the case of figure 6.

Figure 11. Three snapshots of the transport streamfunction, shown in black lines (contour interval is 5 sverdrups), superimposed on colours that show the departures of SST from the time average of figure 1 (the units are °C). Negative values of transport are dashed and correspond to a cyclonic circulation. All fields are periodic in time with a period of 17.7 years, and the times of the snapshots are marked on each panel. The SST anomalies travel clockwise around the anticyclonic gyre (solid contours) taking about thirty-five years to reach the tropics from the mid-latitudes. The longitudinal elongation of the SST anomalies is forced by the heat exchange with an atmosphere that is zonally averaged.

Figure 12. The period of the oscillatory solution as a function of the Rossby wave delay (a), and of the advection time around the subtropical gyre (b). The gyral advection time is defined as $L_x L_y H/\psi_{max}$, where ψ_{max} is the maximum value of the transport streamfunction, ψ. The circles show the computed value of the period when the oscillations are sustained, while the asterisks shows the computed period for oscillations that are damped. In each panel, the solid line is a least squares fit obtained assuming that the period is proportional to the square root of the abscissa.

Figure 13. Zonally average heat transports anomalies and heat storage rate at $y = 5,000$ km during one period of the oscillation. The ONHT lead the ANHT by about 6 years, which is about one third of the period.

Figure 1

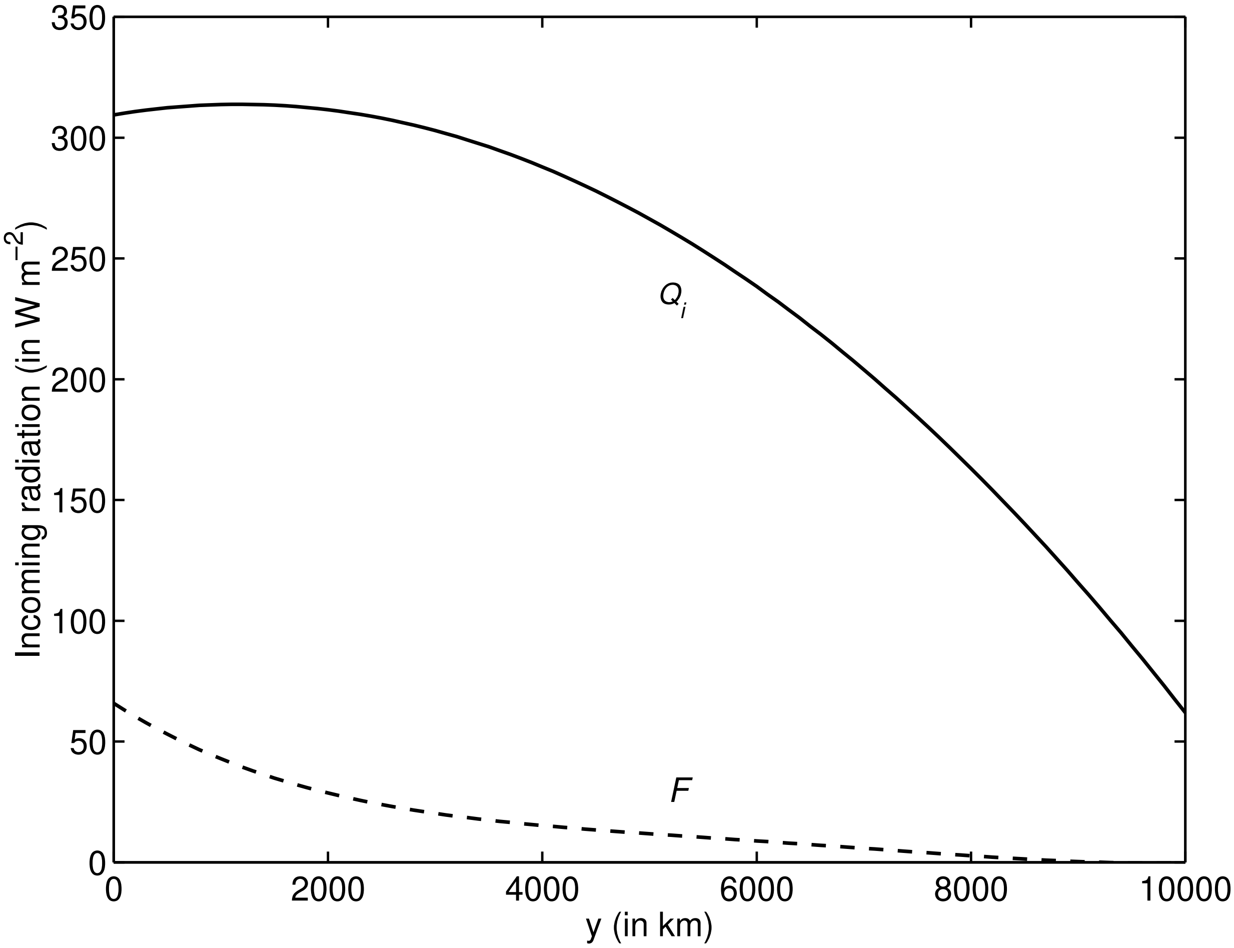

350
300
250
200
150
100
50
0
Incoming radiation (in W m^{-2})
Q_i
F
0
2000
4000
6000
8000
10000
y (in km)

Figure 2

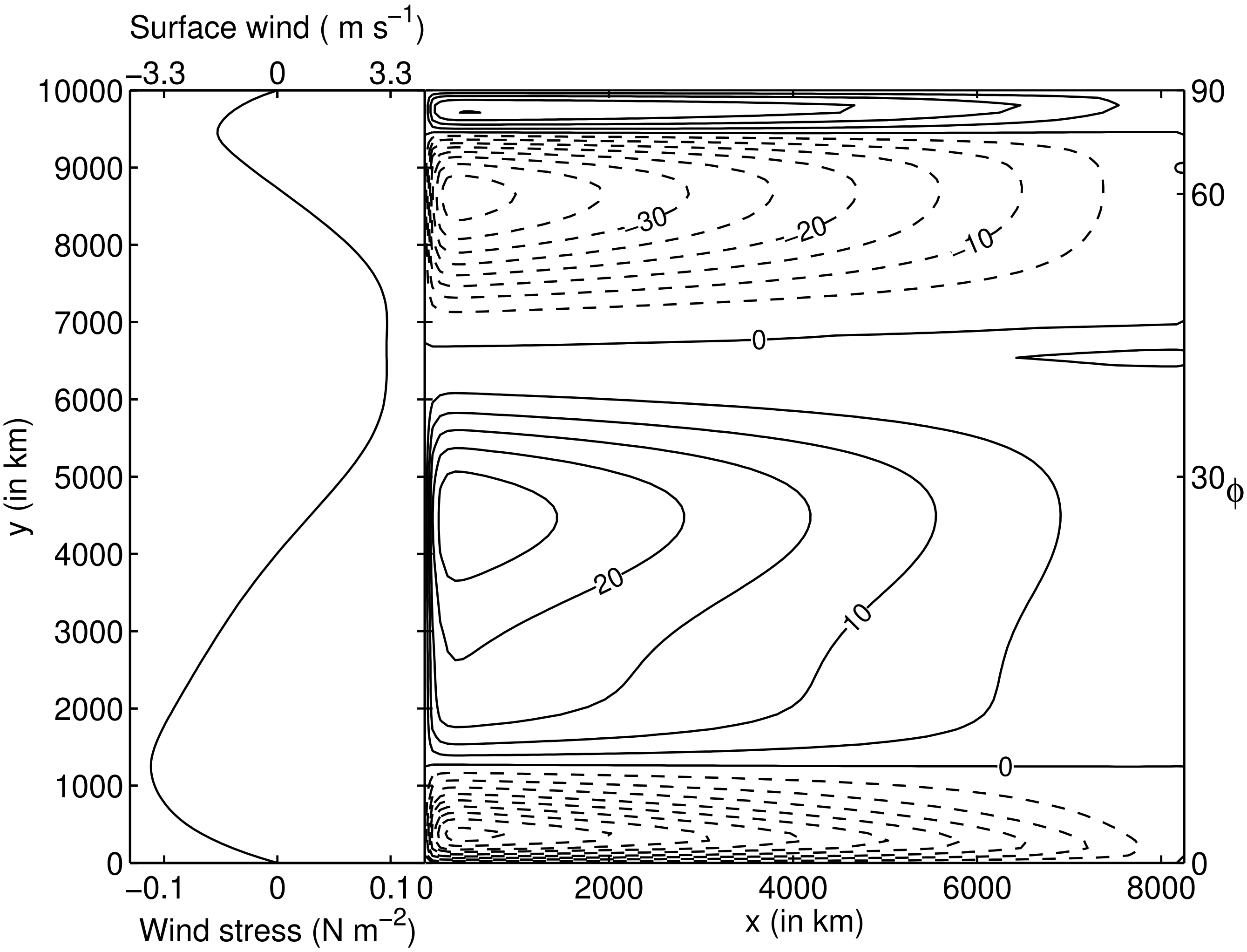

Surface wind (m s^{-1})
–3.3
0
3.3
10000
9000
8000
7000
6000
5000
4000
3000
2000
1000
0
y (in km)
–0.1
0
0.1
Wind stress (N m^{-2})
0
2000
4000
6000
8000
x (in km)
90
60
30
0
ϕ
–30
–20
–10
0
20
10
0

Figure 3

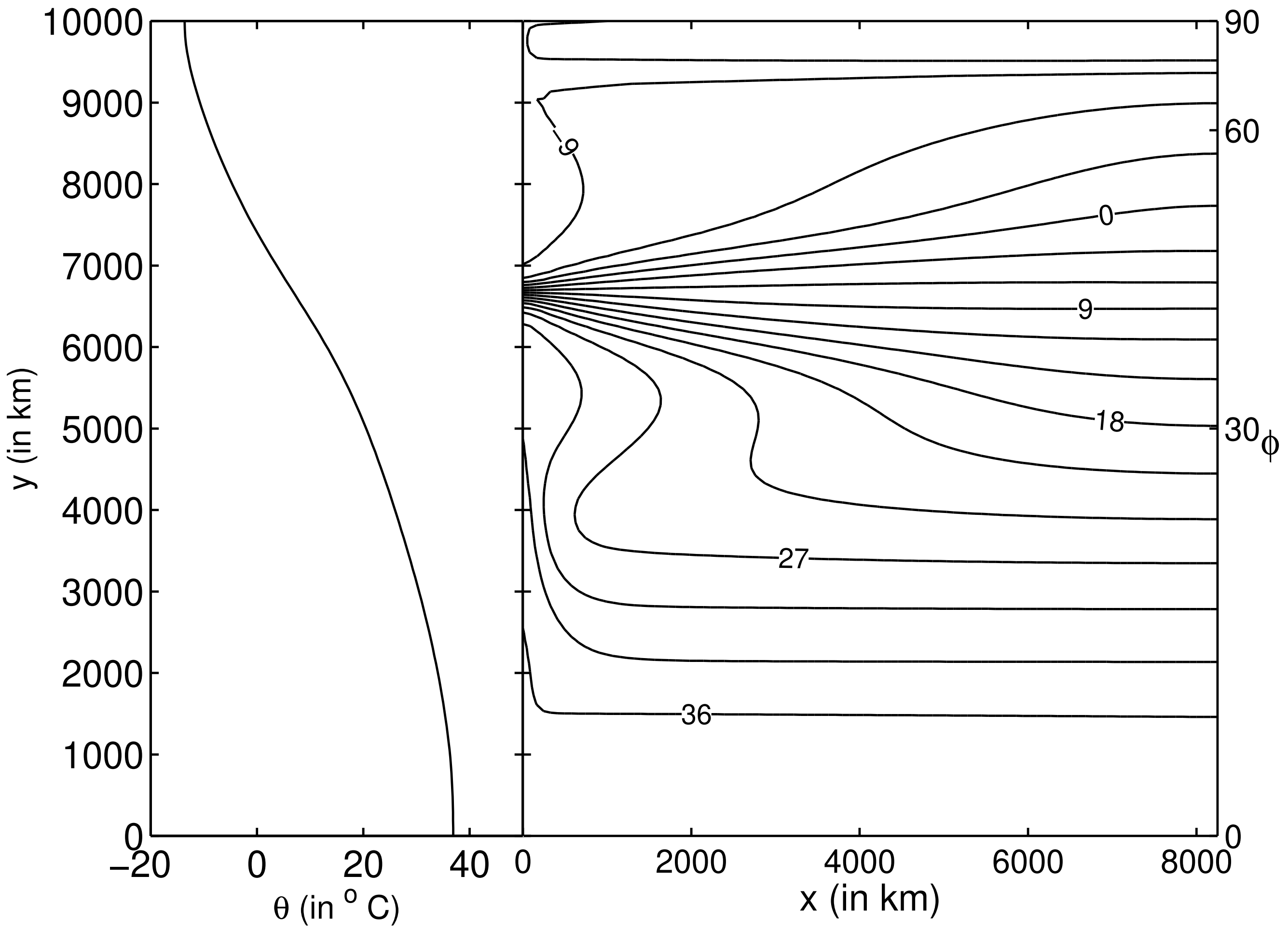
10000
9000
8000
7000
6000
5000
4000
3000
2000
1000
0
y (in km)
−20
0
20
40
θ (in ^{o} C)
0
2000
4000
6000
8000
x (in km)
90
60
30
0
φ
-9
0
9
18
27
36

Figure 4

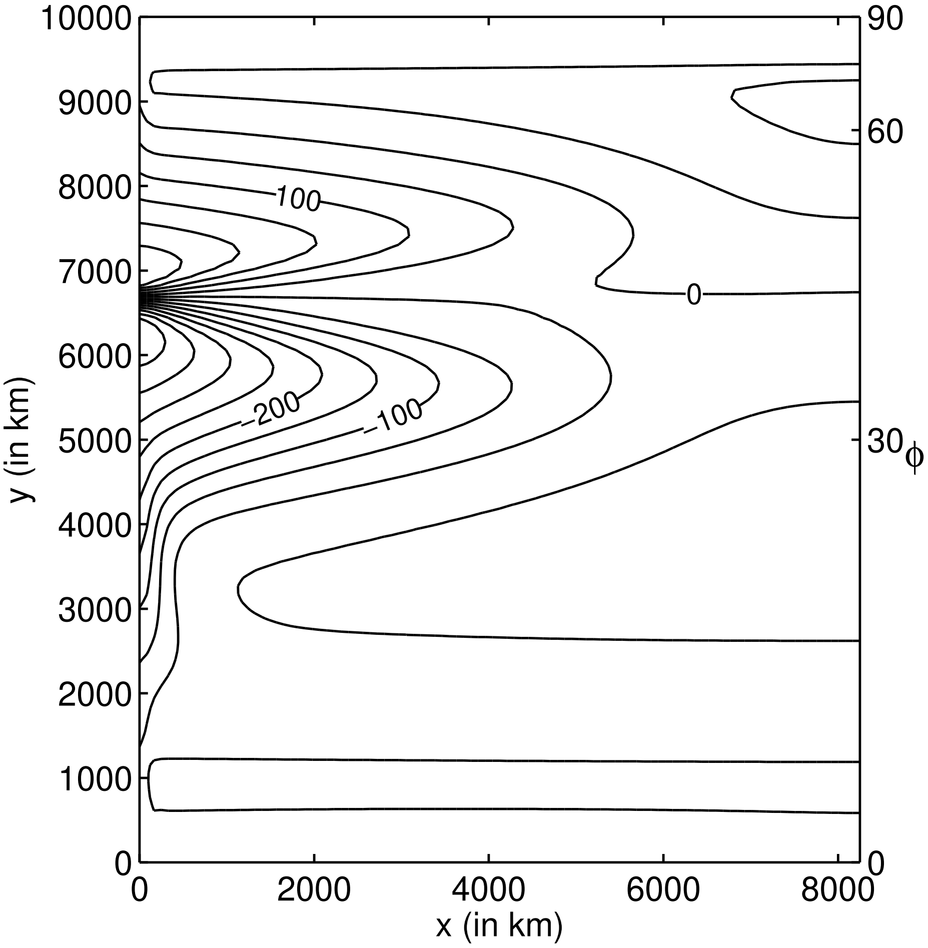

10000
9000
8000
7000
6000
5000
4000
3000
2000
1000
0
90
60
30
0
φ
y (in km)
x (in km)
0
2000
4000
6000
8000
100
0
−200
−100

Figure 5

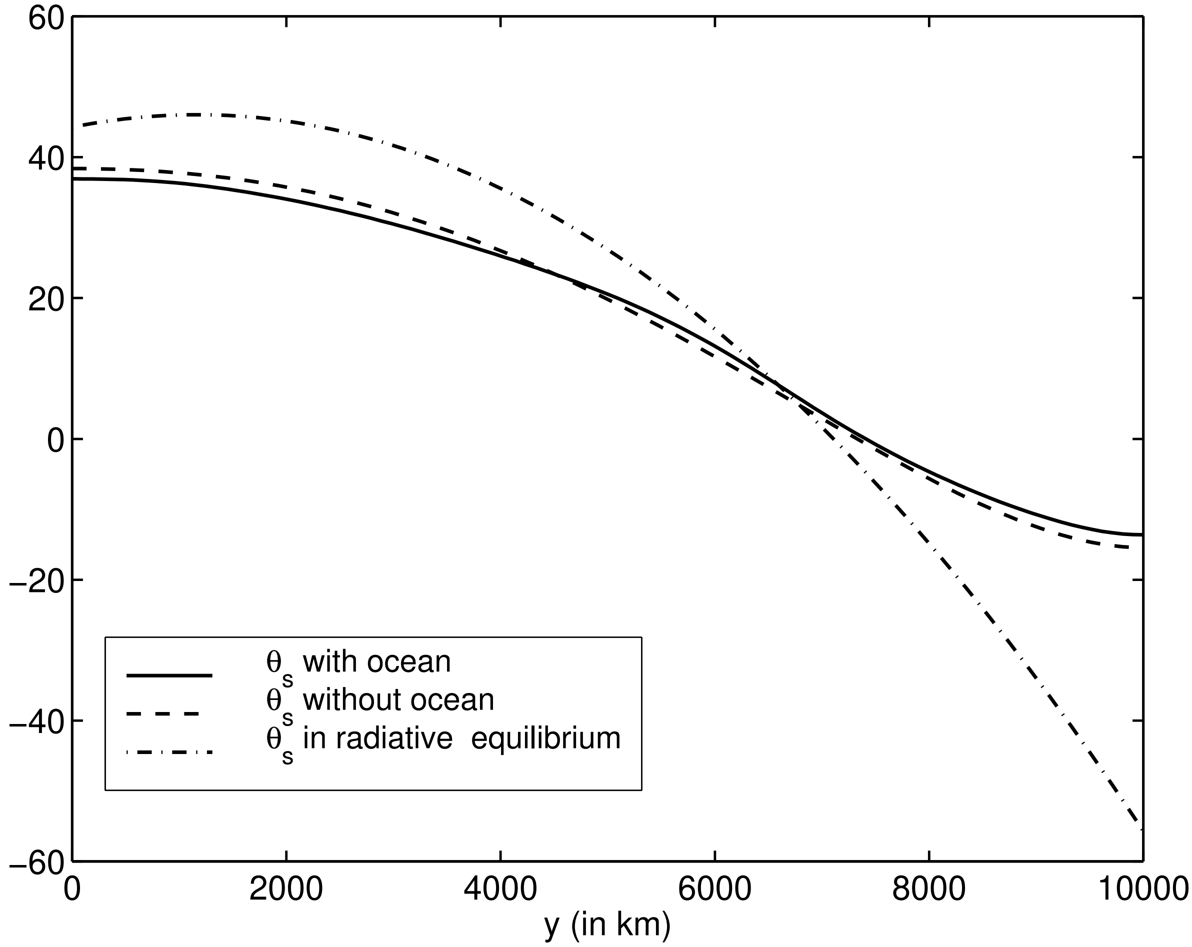

60
40
20
0
−20
−40
−60
0
2000
4000
6000
8000
10000
y (in km)
θ_s with ocean
θ_s without ocean
θ_s in radiative equilibrium

Figure 6

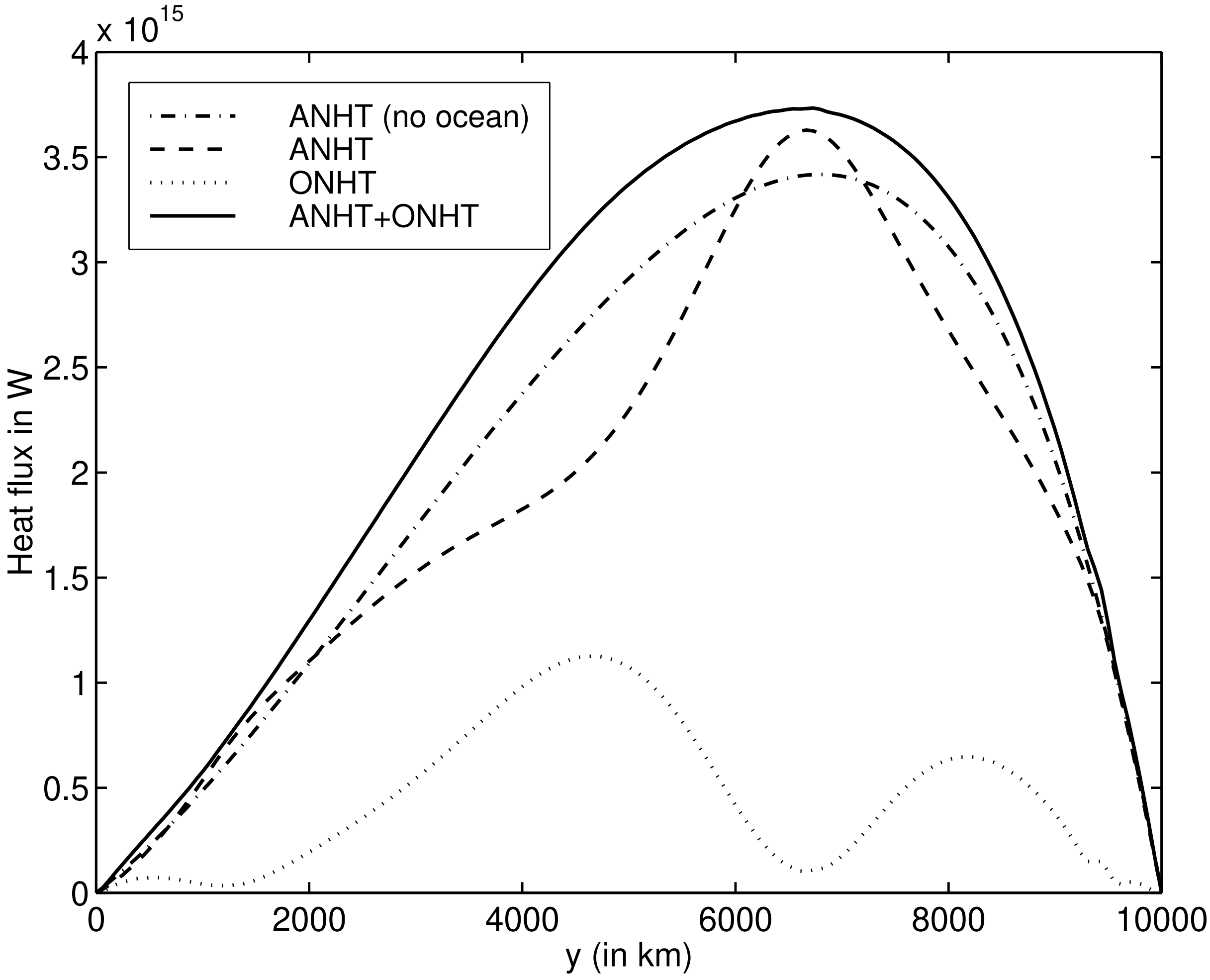
x 10^15
4
3.5
3
2.5
2
1.5
1
0.5
0
Heat flux in W
0
2000
4000
6000
8000
10000
y (in km)
ANHT (no ocean)
ANHT
ONHT
ANHT+ONHT

Figure 7

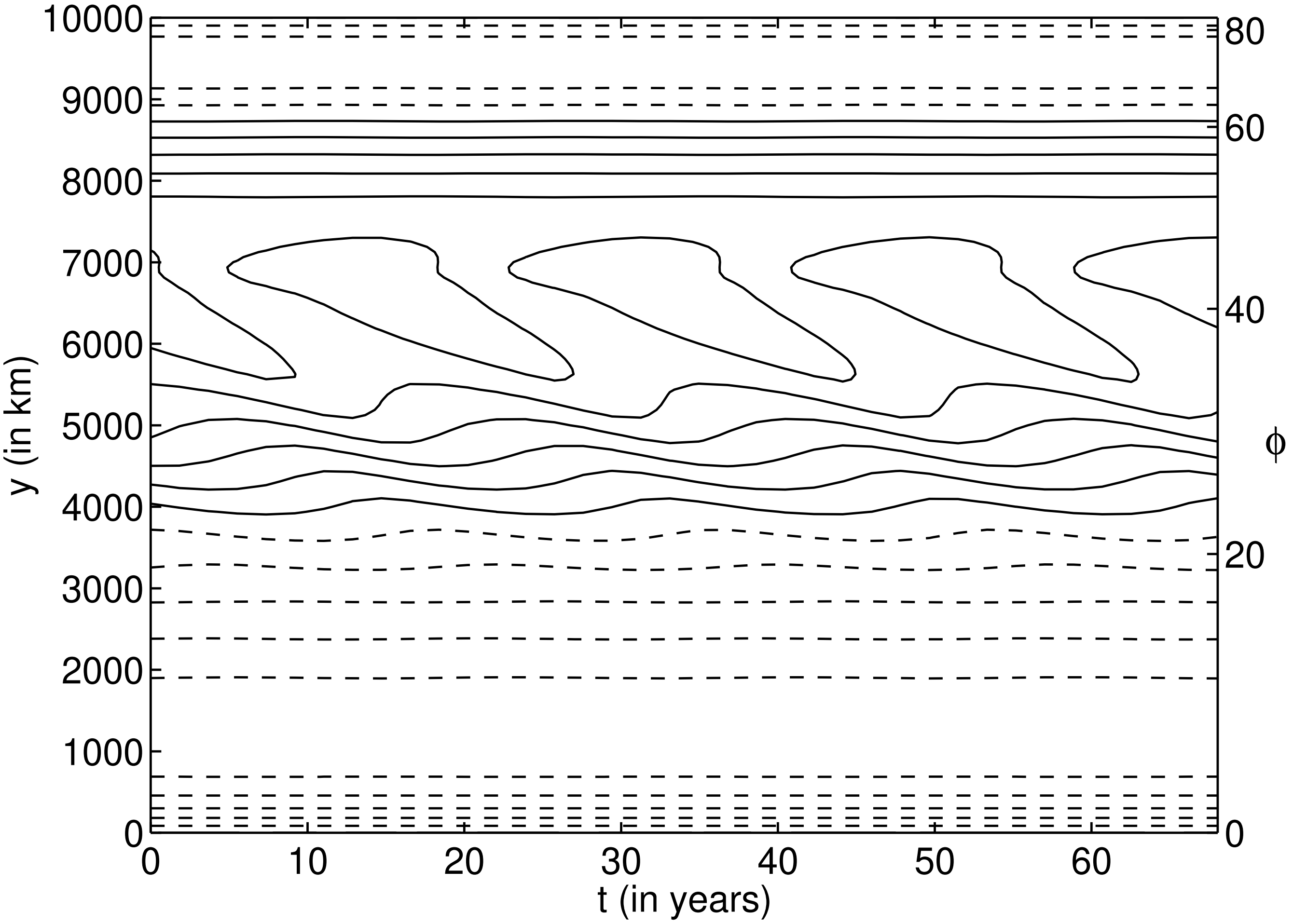

10000
9000
8000
7000
6000
5000
4000
3000
2000
1000
0
y (in km)
0
10
20
30
40
50
60
t (in years)
80
60
40
20
0
ϕ

Figure 8

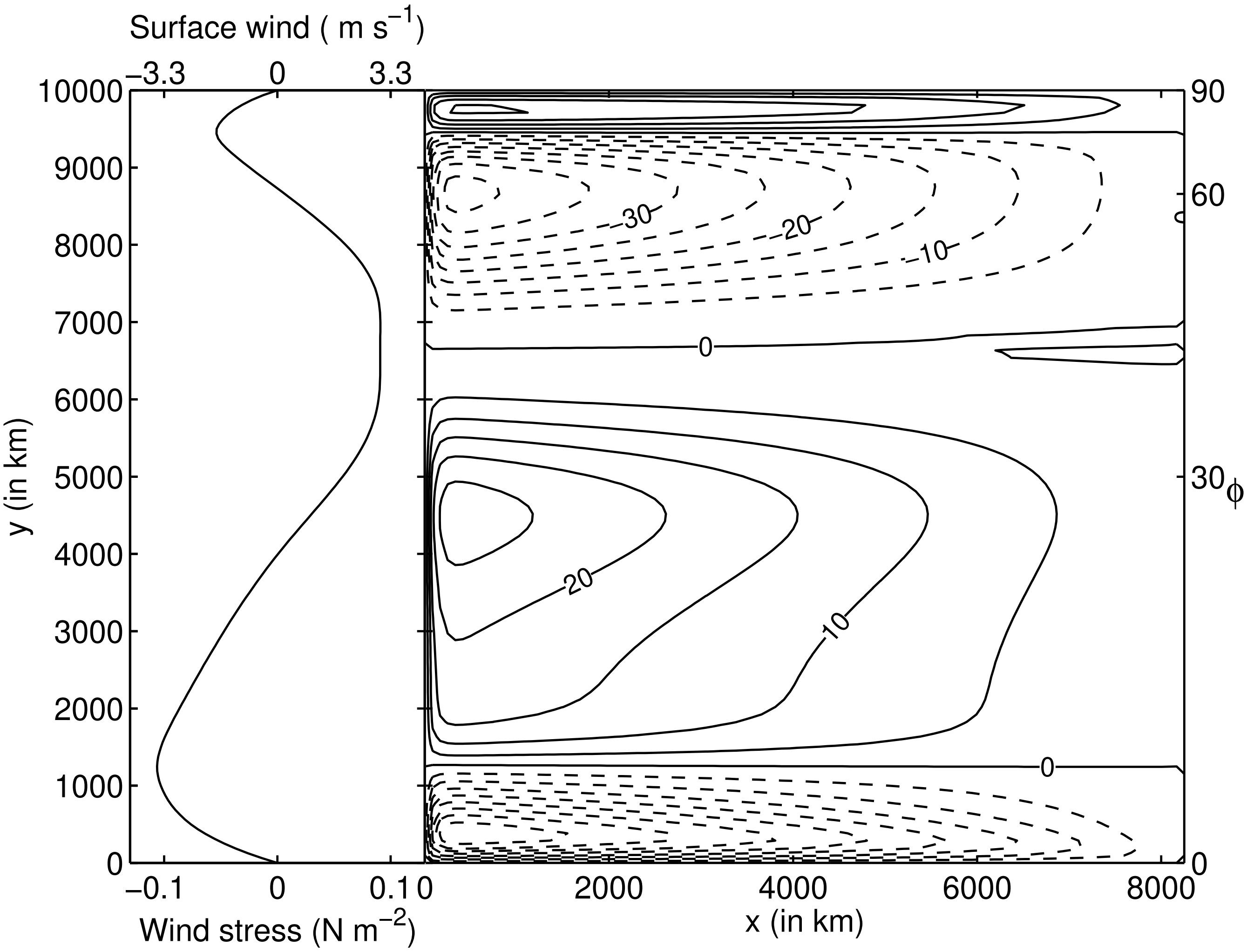

Surface wind (m s^{-1})
–3.3
0
3.3
10000
9000
8000
7000
6000
5000
4000
3000
2000
1000
0
y (in km)
–0.1
0
0.1
Wind stress (N m^{-2})
0
2000
4000
6000
8000
x (in km)
90
60
30
0
ϕ
-30
-20
-10
0
20
10
0

Figure 9

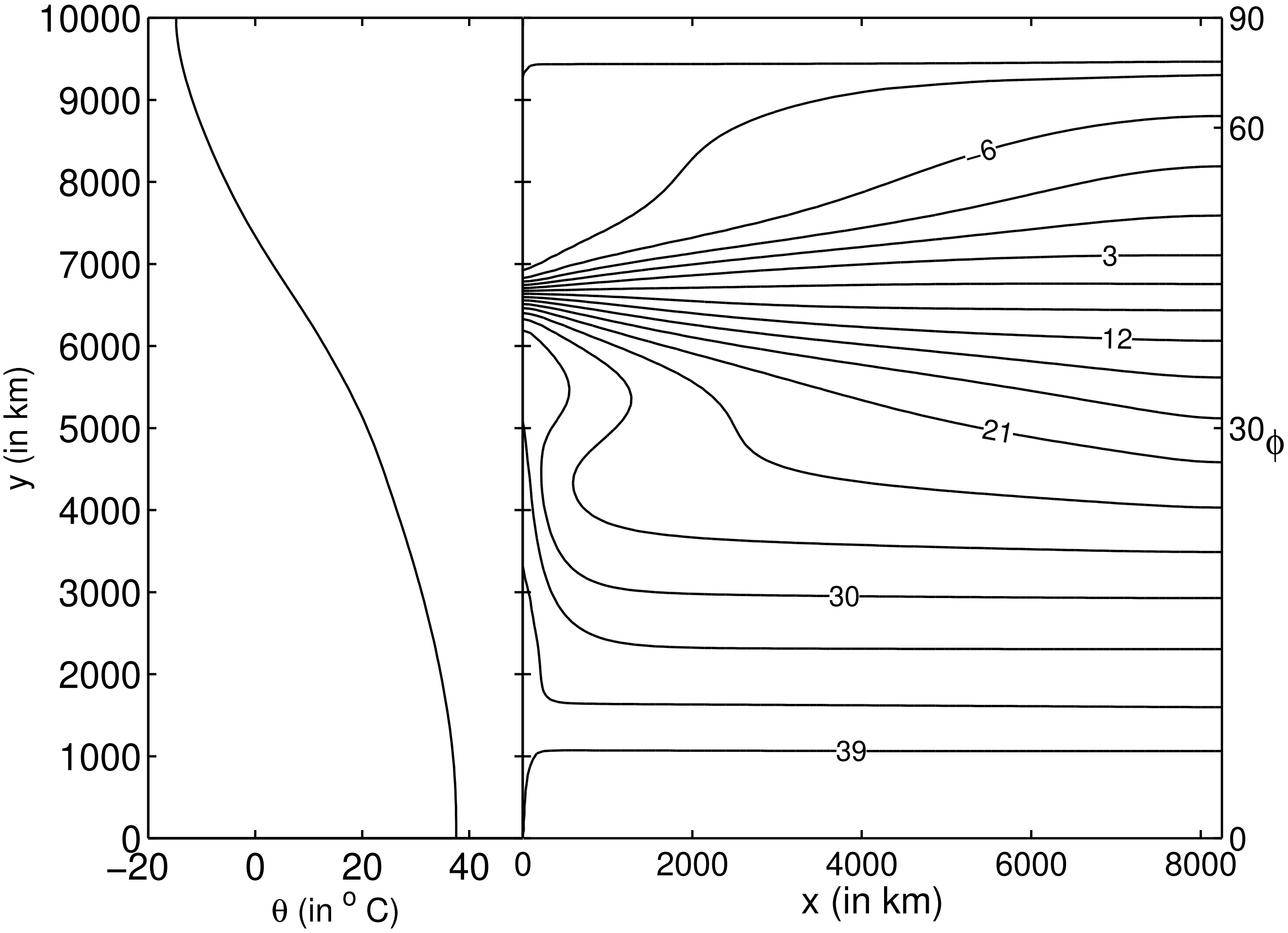

10000
9000
8000
7000
6000
5000
4000
3000
2000
1000
0
y (in km)
−20
0
20
40
θ (in ^{o} C)
0
2000
4000
6000
8000
x (in km)
90
60
30
0
φ
6
3
12
21
30
39

Figure 10

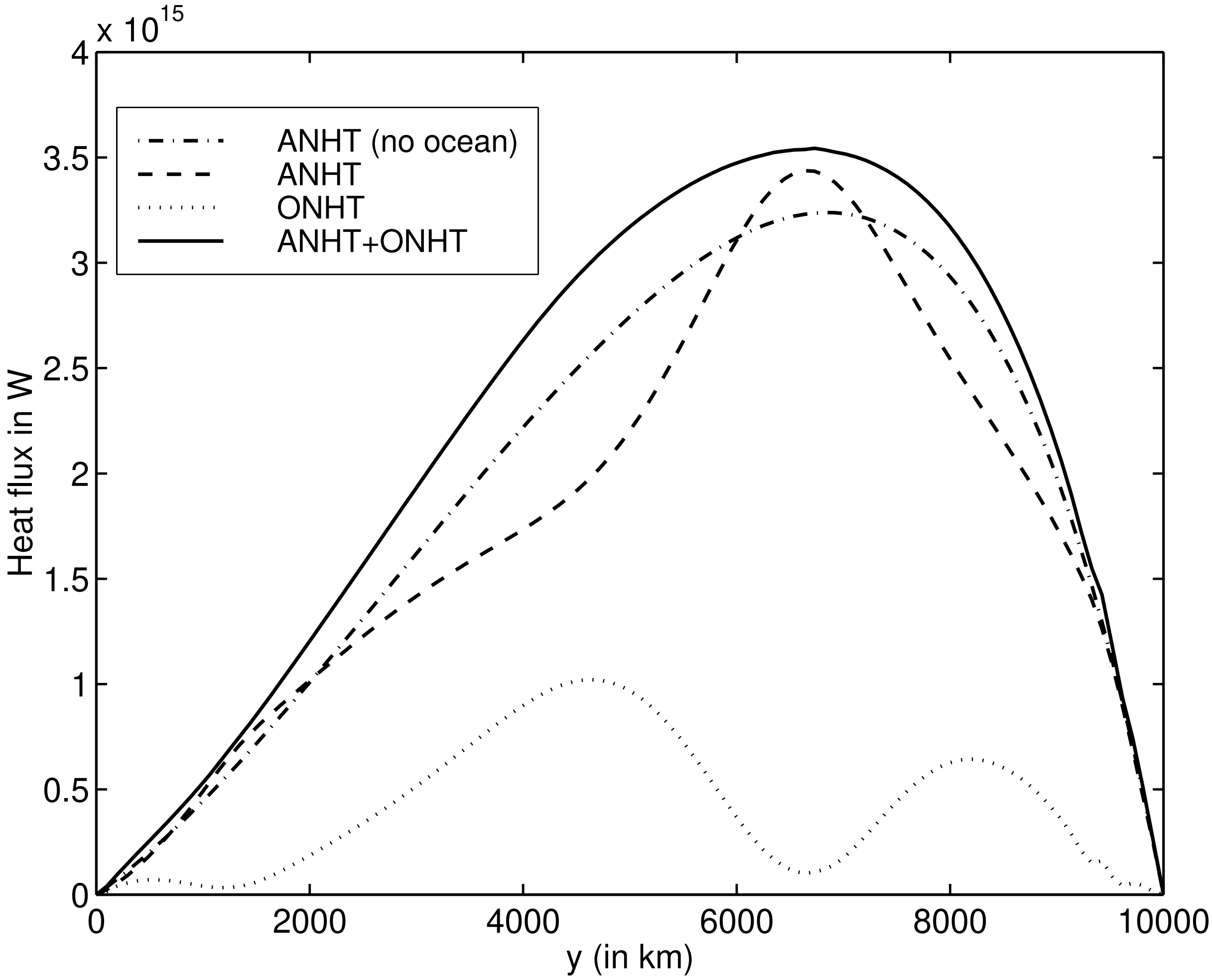
x 10^15
4
3.5
3
2.5
2
1.5
1
0.5
0
Heat flux in W
ANHT (no ocean)
ANHT
ONHT
ANHT+ONHT
0
2000
4000
6000
8000
10000
y (in km)

Figure 11

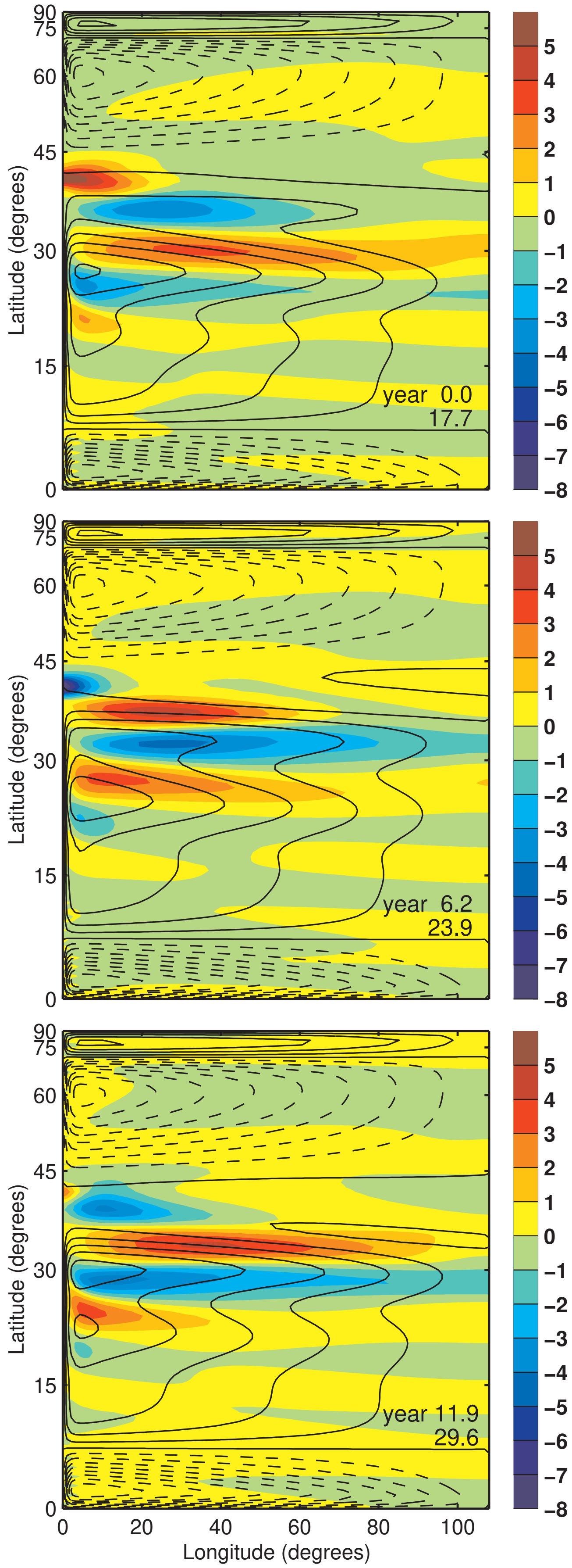

90
75
60
45
30
15
0
Latitude (degrees)
year 0.0
17.7
year 6.2
23.9
year 11.9
29.6
0
20
40
60
80
100
Longitude (degrees)
5
4
3
2
1
0
−1
−2
−3
−4
−5
−6
−7
−8

Figure 12

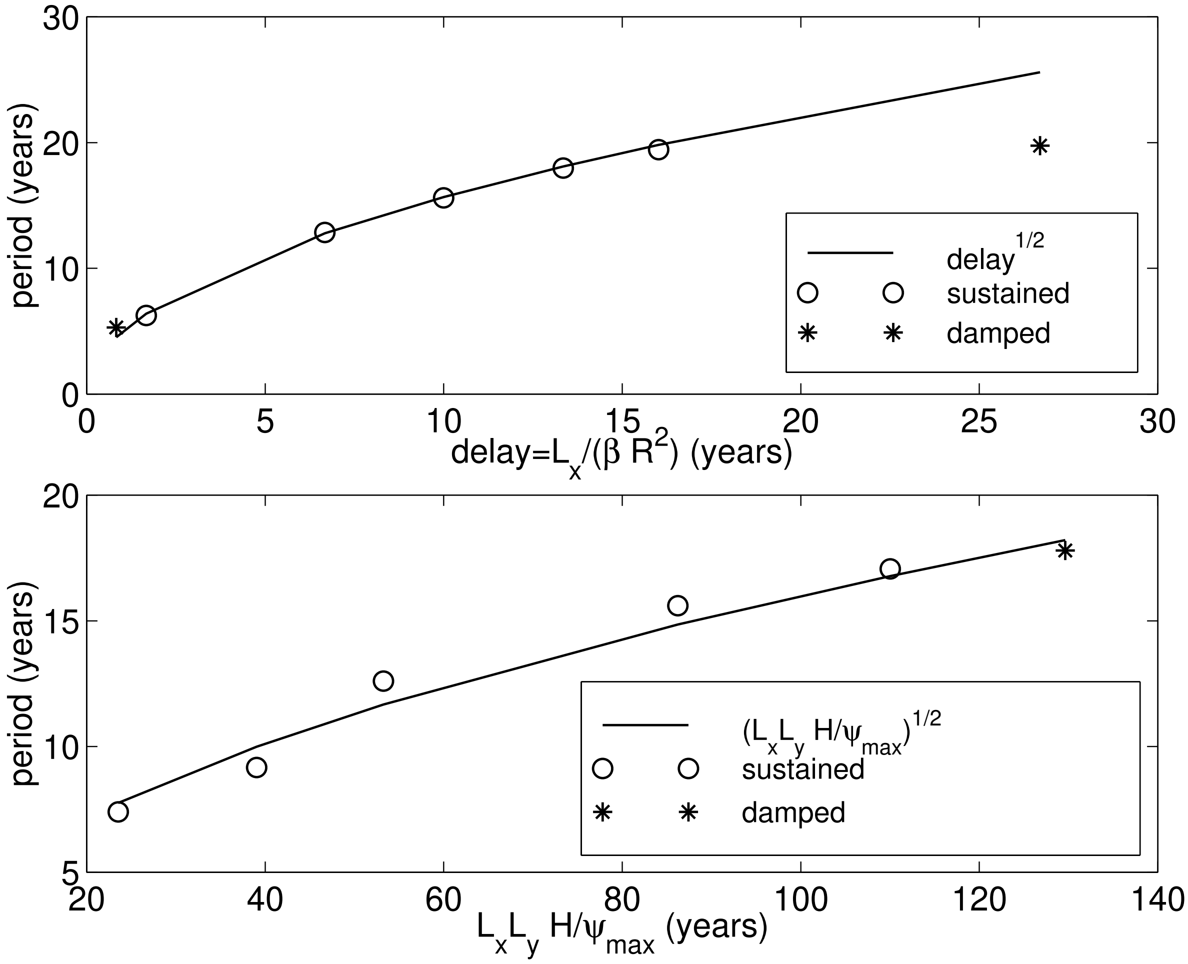

30
20
10
0
period (years)
delay$^{1/2}$
sustained
damped
0
5
10
15
20
25
30
delay=$L_x/(\beta R^2)$ (years)
20
15
10
5
period (years)
$(L_x L_y H/\psi_{max})^{1/2}$
sustained
damped
20
40
60
80
100
120
140
$L_x L_y H/\psi_{max}$ (years)

Figure 13

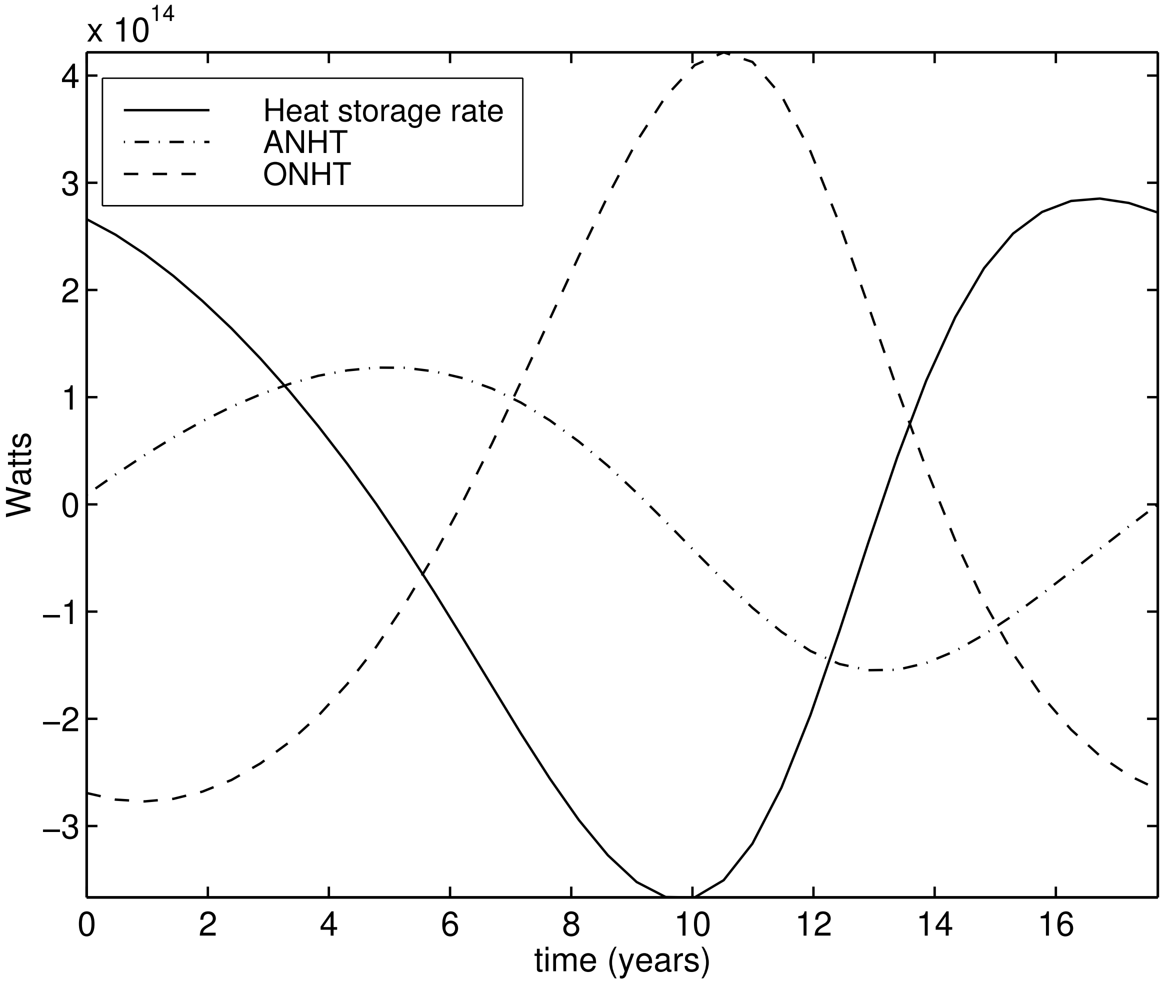

x 10^14
4
3
2
1
0
−1
−2
−3
Watts
Heat storage rate
ANHT
ONHT
0
2
4
6
8
10
12
14
16
time (years)